

# Study of flow behaviors of droplet merging and splitting in microchannels using Micro-PIV measurement

Feng Shen<sup>1</sup> · Yi Li<sup>1</sup> · Zhaomiao Liu<sup>1</sup> · XiuJun Li<sup>2,3</sup> 

Received: 16 November 2016 / Accepted: 16 March 2017 / Published online: 27 March 2017  
© Springer-Verlag Berlin Heidelberg 2017

**Abstract** Droplet merging and splitting are important droplet manipulations in droplet-based microfluidics. However, the fundamental flow behaviors of droplets were not systematically studied. Hence, we designed two different microstructures to achieve droplet merging and splitting respectively, and quantitatively compared different flow dynamics in different microstructures for droplet merging and splitting via micro-particle image velocimetry (micro-PIV) experiments. Some flow phenomena of droplets different from previous studies were observed during merging and splitting using a high-speed microscope. It was also found the obtained instantaneous velocity vector fields of droplets have significant influence on the droplets merging and splitting. For droplet merging, the probability of droplets coalescence ( $\eta$ ) in a microgroove is higher

( $50\% < \eta < 92\%$ ) than that in a T-junction microchannel ( $15\% < \eta < 50\%$ ), and the highest coalescence efficiency ( $\eta = 92\%$ ) comes at the two-phase flow ratio  $e$  of 0.42 in the microgroove. Moreover, compared with a cylinder obstacle, Y-junction bifurcation can split droplets more effectively and the droplet flow during splitting is steadier. The results can provide better understanding of droplet behaviors and are useful for the design and applications of droplet-based microfluidics.

**Keywords** Droplet-based microfluidics · Droplet merging · Droplet splitting · Velocity vector field · Micro-particle image velocimetry (Micro-PIV)

## 1 Introduction

Droplet-based microfluidics has attracted more and more research attentions (Dou et al. 2016; Baroud et al. 2010; Chen et al. 2015; Wu et al. 2015; Whitesides 2006) and has very significant potential for material science applications and chemical and biological applications (Sharma et al. 2013; Seemann et al. 2012; Schneider et al. 2013; Rosenfeld et al. 2014; Chou et al. 2015). Taking advantage of flow dynamics of microdroplets in microchannels (Stone et al. 2004), microdroplets can provide unique physical and chemical contrasts with the outer medium (Baroud et al. 2010). Therefore, the droplet-based microfluidics has many advantages, such as high throughput, low cost, small sample volumes (2–4 nL), precise control of reagent composition, fast mixing, and minimal contamination (Leman et al. 2015; Lin and Qin. 2008; Li et al. 2012; Shen et al. 2015a, b). So far, its applications have rapidly advanced to a broad range of chemical and biological assays such as droplet-based cell screening

This article is part of the topical collection “2016 International Conference of Microfluidics, Nanofluidics and Lab-on-a-Chip, Dalian, China” guest edited by Chun Yang, Carolyn Ren and Xiangchun Xuan.

**Electronic supplementary material** The online version of this article (doi:10.1007/s10404-017-1902-y) contains supplementary material, which is available to authorized users.

✉ Feng Shen  
shenfeng@bjut.edu.cn

✉ XiuJun Li  
xli4@utep.edu

- <sup>1</sup> College of Mechanical Engineering and Applied Electronics Technology, Beijing University of Technology, Beijing 100124, China
- <sup>2</sup> Department of Chemistry, University of Texas at El Paso, El Paso, TX 79968, USA
- <sup>3</sup> Border Biomedical Research Center, University of Texas at El Paso, El Paso, TX 79968, USA

and diagnostics (Schoeman et al. 2014; Mark et al. 2010; Mu et al. 2013; Qi et al. 2012; Yeo et al. 2011; Gijs et al. 2010), drug delivery (Yang et al. 2015), single-molecule investigations (Dutse and Yusof 2011; Mai et al. 2012), and microreactors (Dou et al. 2016; Marques and Fernandes 2011; Sun et al. 2013).

Different strategies have been developed for microdroplet manipulations (Day et al. 2012; Fatoyinbo and Labeed 2015), such as microdroplet generation (Wu et al. 2009; Wang et al. 2010; Chong et al. 2016), merging (Gu et al. 2011; Wu et al. 2014; Pit et al. 2015), splitting (Christopher et al. 2009; Pit et al. 2015), injecting (Abate et al. 2010), mixing (Song et al. 2003) and sorting (Schmid et al. 2014; Salánki et al. 2014). However, the microdroplet flow behaviors during these manipulations are complex due to the deformable interface of the microdroplets and the variations of interfacial tension (Liu et al. 2007; Christopher et al. 2009; Baroud et al. 2010; Huerre et al. 2015; Wang et al. 2015a, b). In order to control the flow behaviors of microdroplets in a controlled and reproducible manner (Baroud et al. 2010; Stone et al. 2004), these fluid dynamical behaviors should be well understood (Seemann et al. 2012; Nghe et al. 2011; Schoch et al. 2008; Woerner 2012; Squires and Quake 2005).

Droplets merging and splitting are regarded as two critical manipulations in droplet-based microfluidics, because coalescence is an effective method to mix reagents and induce chemical and biological reactions in microfluidics devices (Gu et al. 2011; Teh et al. 2008; Wu et al. 2014; Pit et al. 2015; Jin et al. 2010), while splitting plays an important role in diluting, concentrating or separating particles in a droplet (Pit et al. 2015; Teh et al. 2008; Wang et al. 2015a, b; Sun and Liu 2013). Several methods have been developed to achieve droplet merging and splitting, which can be generally categorized as active (Zagnoni et al. 2009; Wang et al. 2009; Jung et al. 2015; Xu et al. 2012; Sesen et al. 2014) and passive (Wang et al. 2013a; Simon and Lee 2012; Niu et al. 2008) methods. Passive methods are generally flow-induced and based on geometry-mediated mechanisms (Christopher et al. 2009; Zhou et al. 2015; Wang et al. 2014). It has been demonstrated that droplet merging can be achieved by using flow resistance structures (Xu et al. 2011; Tan et al. 2004), micro column structures (Niu et al. 2008), T-junction structures (Christopher et al. 2009; Yang et al. 2012), Y-junction structures (Wang et al. 2013b), cross-shaped junctions (Wang et al. 2013a), and so on. Meanwhile, microdroplet splitting can be obtained at precise locations such as 3D crossing microstructures (Chen et al. 2012, 2016), T-shaped junction (Tan et al. 2004; Yoon et al. 2013; Hoang et al. 2013; Link et al. 2004), branching channels (Moritani et al. 2011; Zhou et al. 2015), and artificial obstacle inside channels (Chung et al. 2010; Li et al. 2014; Protière et al.

2010). Taking advantage of fluid dynamics in elaborately designed microchannels, the passive methods require no electrodes and have advantages of low contamination of inter-droplet (Wang et al. 2013a; Simon and Lee 2012). Therefore, better understanding of the microdroplet flow characteristics is particularly important for passive methods of droplet manipulations.

Many studies have recently attempted to reveal the fluid dynamical mechanisms of droplets merging and splitting by investigating the variations of interfacial tension along the drop surface (Baroud et al. 2010; Seemann et al. 2012; Nghe et al. 2011; Woerner 2012; Christopher et al. 2009). Droplets merging is mainly driven by the interfacial tension of droplets and can be realized by overcoming the interfacial tension and leading the interface unstable (Baroud et al. 2010; Christopher et al. 2009). Liquid film drainage theory and capillary number ( $Ca = \mu U/\sigma$ , where  $\mu$  is generally the dynamic viscosity of the most viscous fluid in the two-phase system,  $U$  is the velocity of that phase, and  $\sigma$  is the interfacial tension), representing the relative magnitude of viscous stress and interfacial tension, have been used to characterize the coalescence process of millimeter-scaled droplet pairs (Loewenberg and Hinch 1997; Yoon et al. 2005). On the contrary, splitting of droplets depends on the droplet size, capillary number and the geometry of the microchannels (Pit et al. 2015; Leshansky and Pismen 2009; Collignon et al. 2015; Moritani et al. 2011; Deng et al. 2011). Splitting occurs at a low capillary number, when passing through a circular cylinder in a microchannel. Short droplets break up as the capillary number increases, while long droplets do not break up (Chung et al. 2009). Most of previous studies mainly focused on the droplet interface deformation and interfacial tension using microscope observations. However, relatively few studies have focused on droplet behaviors during merging and splitting in microchannels, in which droplets controlled by the surrounding viscous liquid, can deform significantly on accounting of the confining boundaries (Christopher et al. 2009; Choi and Lee 2014; Gu et al. 2011), leading to series of new fluid dynamics problems such as the change of the interfacial tension and nonlinear problems of droplets (Baroud et al. 2010; Raven and Marmottant 2006; Guillot et al. 2008; Chen et al. 2011).

Recently, in order to understand the effect of the droplet's internal circulation on mass transfer rates during the formation and deformation of droplets (Duxenneuner et al. 2014; Timgren et al. 2008; Dore et al. 2012; Alves et al. 2005), a number of publications investigated the internal flow pattern of liquid slugs or droplets moving slowly along the microchannel using either micro-scale particle image velocimetry (micro-PIV) (Lindken et al. 2009; Kinoshita et al. 2007; Oishi et al. 2011;

Dietrich et al. 2008) or numerical simulation (Yan et al. 2013; Sarrazin et al. 2006; Shen et al. 2014). However, there are only a few qualitative visualization studies on the velocity vector field of microdroplets during merging and splitting using micro-PIV (Wang et al. 2013a, b; Liu et al. 2015; Jin and Yoo 2012). Systematic quantitative studies for better understanding of the fluid dynamic characteristics of microdroplet merging and splitting are needed.

Herein, we proposed two different microstructures to achieve droplet merging and splitting and then compared different flow dynamics in these two different microstructures via micro-PIV and high-speed microscopy to investigate fundamental flow characteristics of droplet merging and splitting. We first used a T-junction channel to achieve the first step of coalescence and a rectangular microgroove to increase the coalescence efficiency. Meanwhile, two obstacle structures, namely a cylinder obstruction and a Y-junction bifurcation, were used to induce the splitting of microdroplets, respectively. Different forms of merging and splitting of microdroplets were observed in the experiments, including five different coalescence forms in the T-junction microchannel, two different coalescence forms in microgroove, four different splitting forms induced by the cylinder obstruction, and two splitting forms induced by the Y-junction bifurcation. The influence of two-phase flow ratios ( $e$ ) on the coalescence efficiency ( $\eta$ ) was also studied. Moreover, velocity vector fields of microdroplets during different forms of merging and splitting in different microchannel structures were investigated using a micro-PIV system. This study focuses on the microdroplet behaviors and the velocity vector fields, which have fundamental and practical significance to the design and applications of droplet-based microfluidics.

## 2 Methods

### 2.1 Microfluidic chips

The layouts of these two microfluidic chips are illustrated in Fig. 1. Both of them have a T-shaped junction and a rectangular microgroove to increase the chance of droplet merging. Usually, the microdroplets for merging should arrive at the T-shaped junction at the same time, and the contact time of microdroplets is very short. However, due to the two-phase flow characteristics in microchannel and other uncontrollable factors of microdroplets transportation, etc., the synchronism of microdroplets is hard to maintain in the actual operating process, especially for the head-on collision of microdroplets at a T-shaped junction (Wang et al. 2013a). Therefore, T-shaped junction cannot ensure efficient merging of microdroplets and adding a rectangular microgroove can avoid the synchronism problem and increase the chance of microdroplets merging. To achieve microdroplet splitting, a circular cylinder obstacle and a T-shaped bifurcation are designed in chip I (Fig. 1a) and chip II (Fig. 1b), respectively. Although both of the two obstacle structures can achieve microdroplet splitting, their mechanisms are different.

The microfluidic chip I is 21.3 mm in length and 9.1 mm in width, as shown in Fig. 1a. The entrance length of continuous and disperse phases are  $L_1 = 2000 \mu\text{m}$ . In Fig. 1a,  $L_2 = 4.5 \text{ mm}$ ,  $L_3 = 5 \text{ mm}$ ,  $L_5 = 6 \text{ mm}$ . The length and width of the rectangular microgroove are  $L_4 = 2 \text{ mm}$ ,  $W_2 = 500 \mu\text{m}$ , respectively. The width of droplet generation channel and the main channel are  $W_1 = 300 \mu\text{m}$ ,  $W_3 = 500 \mu\text{m}$ , respectively. The diameter of the circular cylinder obstacle is  $300 \mu\text{m}$ . In Fig. 1b, the microfluidic chip II is 16.9 mm in length and 9.1 mm in width. Different from Chip I,  $L_6 = 5 \text{ mm}$ ,  $L_7 = 3 \text{ mm}$ ,  $W_4 = 300 \mu\text{m}$ , and

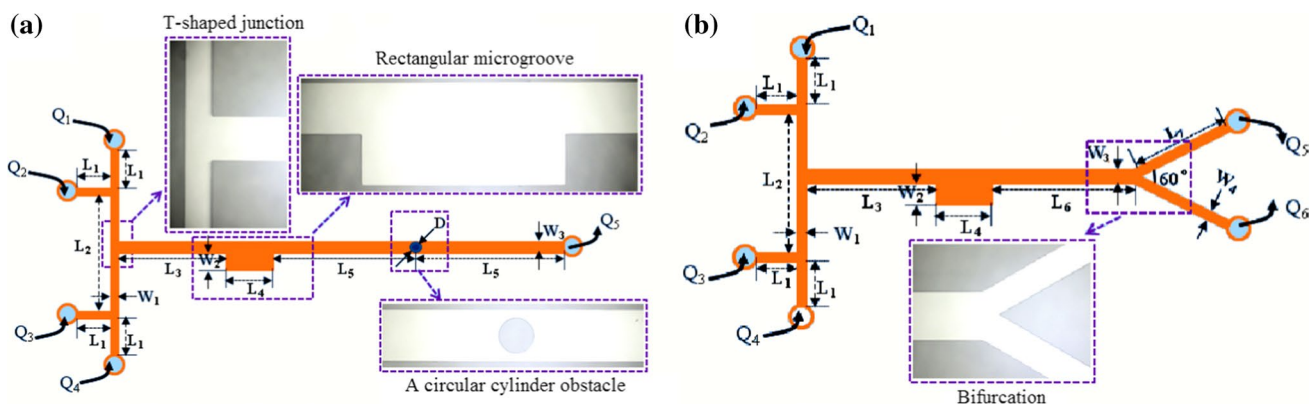


**Fig. 1** Microfluidic chips for merging and splitting of microdroplets. **a** Chip I with a circular cylinder obstacle. **b** Chip II with a Y-shaped bifurcation

the bifurcation angle is  $60^\circ$ . The depth of the microchannel is  $200\ \mu\text{m}$ . Inlet 1 ( $Q_1$ ) and inlet 4 ( $Q_4$ ) are for continuous phases injection, while inlet 2 ( $Q_2$ ) and inlet 3 ( $Q_3$ ) are for the dispersed phases of injection. The microfluidic chips were made of polydimethylsiloxane (PDMS) using a standard soft lithographic method (Duffy et al. 1998; Dou et al. 2014).

## 2.2 Experimental setup

In the experiments, deionized water ( $\rho = 10^3\ \text{kg/m}^3$  and  $\mu = 10^{-3}\ \text{Pa}\cdot\text{s}$ ) (inlet 2) and ethanol (inlet 3) were used as disperse phases, while sunflower oil (inlet 1 and 4) with a density of  $920\ \text{kg/m}^3$ , a viscosity of  $8\ \text{mPa}\cdot\text{s}$  and interfacial tension of  $42.2\ \text{mN/m}$  was used as the continuous phase at the room temperature of  $25\ ^\circ\text{C}$ . Because it was difficult to see the microchannel wall clearly when the silicone oil flowed through microchannels in our experiments, we used the silicone oil mixed with Oil Red O (Sigma-Aldrich Co., USA) to flow through microchannels for 10 min. Then, when we used a microscope to observe the microchannel, we found the microchannel wall could be observed clearly. Considering that Sunflower oil could provide better color contrast, we chose sunflower oil as the continuous phase, as previously reported (Zhou et al. 2015). In this study,  $Q_C$  is the continuous phase flow rate and  $Q_d$  is the dispersed phase flow rate. The two-phase flow ratio is defined as  $e = Q_d/Q_C$ . In order to control the generation rate and the size of microdroplets and realize the microdroplet coalescence and splitting, different flow rates ( $Q_d$  and  $Q_C$ ) were used.

As shown in Fig. 2, a high-speed microscope system (Keyence, VW-9000) was used to record the movement and deformation of microdroplets during different forms of merging and splitting, while a micro-PIV system was employed to obtain the velocity vector fields of microdroplets using tracer particles with a diameter of  $0.71\ \mu\text{m}$

(Thermal Fisher) (Fig. 2b). Details of the micro-PIV system (Dantec Dynamics) were introduced in our previous studies (Shen et al. 2014; Liu et al. 2015). In brief, the particle images were first captured with a resolution of  $1344 \times 1024$  pixels, at a rate of 20 frames per second (fps) with the exposure time of  $80\text{--}600\ \mu\text{s}$  according to the flow rate, and then recorded on a computer for PIV analyses using Dynamic Studio software (Dantec Dynamics V3.40). The acquired particle images were analyzed with an adaptive cross-correlation (ACC) algorithm. The interrogation area was  $16 \times 16$  pixel (50% overlap). Furthermore, the least squares Gauss fitting algorithm was used to detect the peak on the correlation plane to reduce measurement uncertainty and to improve the signal-to-noise ratio.

## 3 Results and discussion

### 3.1 Microdroplet merging in a T-junction

In order to make the two microdroplets contact each other at the T-junction, they should arrive at the T-junction synchronously and the difference of arriving times should be as short as possible. However, in the experiments, it is difficult to make sure that they arrive at the T-junction at the same time. Hence, in order to realize the coalescence of microdroplets, the flow rates must be controlled accurately. According to the difference of the arriving time of microdroplets, the microdroplet merging phenomena have five different forms approximately, as shown in Fig. 3. Figure 3a, b shows that two microdroplets arrived at the T-junction nearly at the same time and had good time synchronicity. Under the pressure of the surrounding fluid, the two microdroplets deformed significantly and squeezed the liquid film between them. After about 1 ms, the liquid film was drained out and coalescence occurred. This squeeze-induced coalescence of deformed microdroplets at

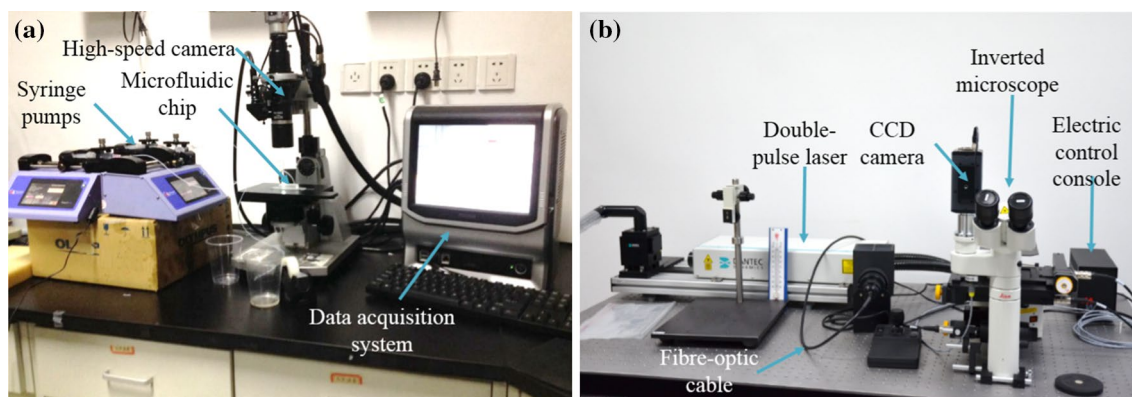


**Fig. 2** Photographs of the experimental setup. **a** High-speed microscope system. **b** Micro-PIV system

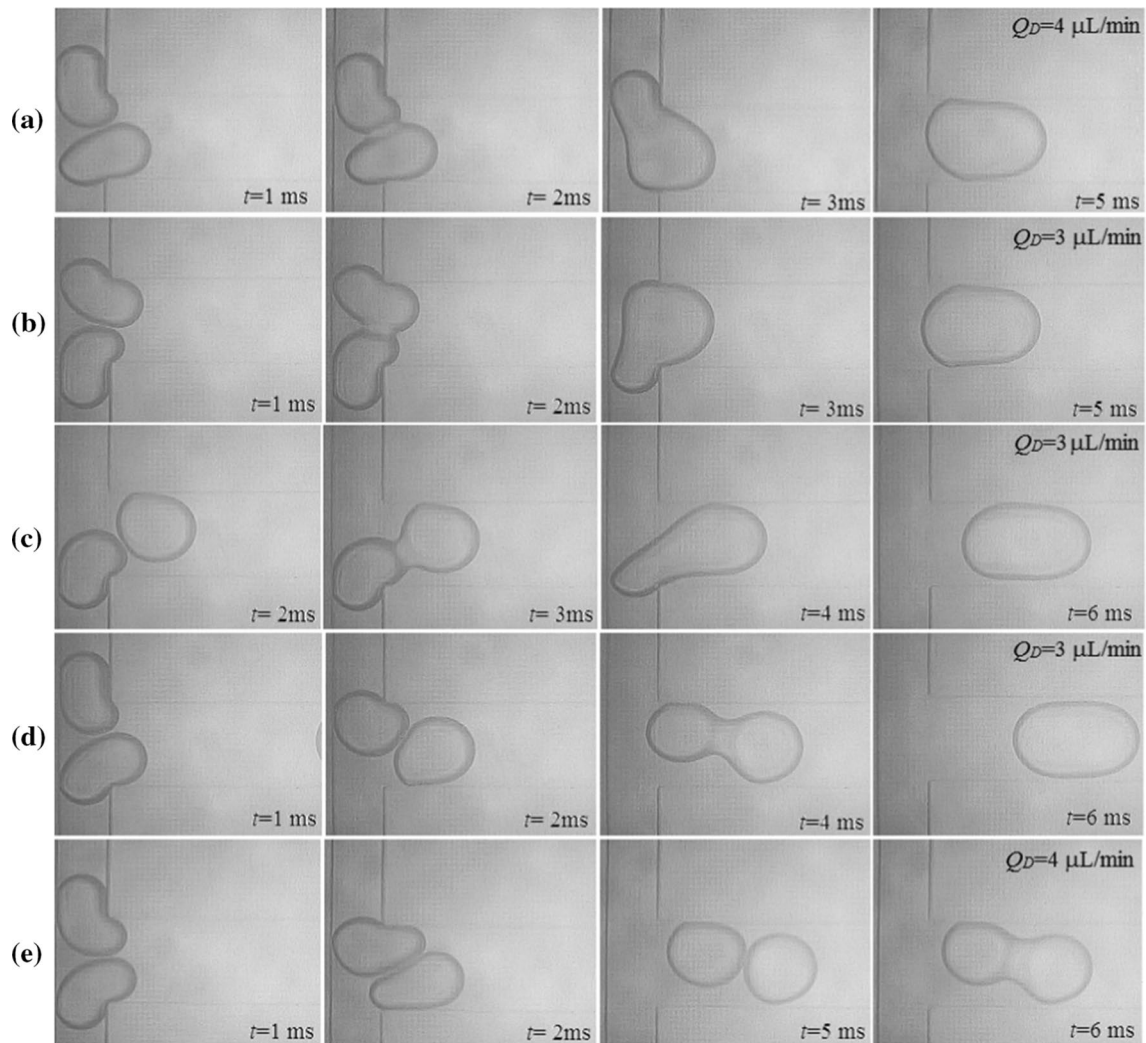


**Fig. 3** Five different forms of microdroplet coalescences at T-junction microchannel at  $Q_C = 10 \mu\text{L}/\text{min}$ . The scale bar is  $300 \mu\text{m}$

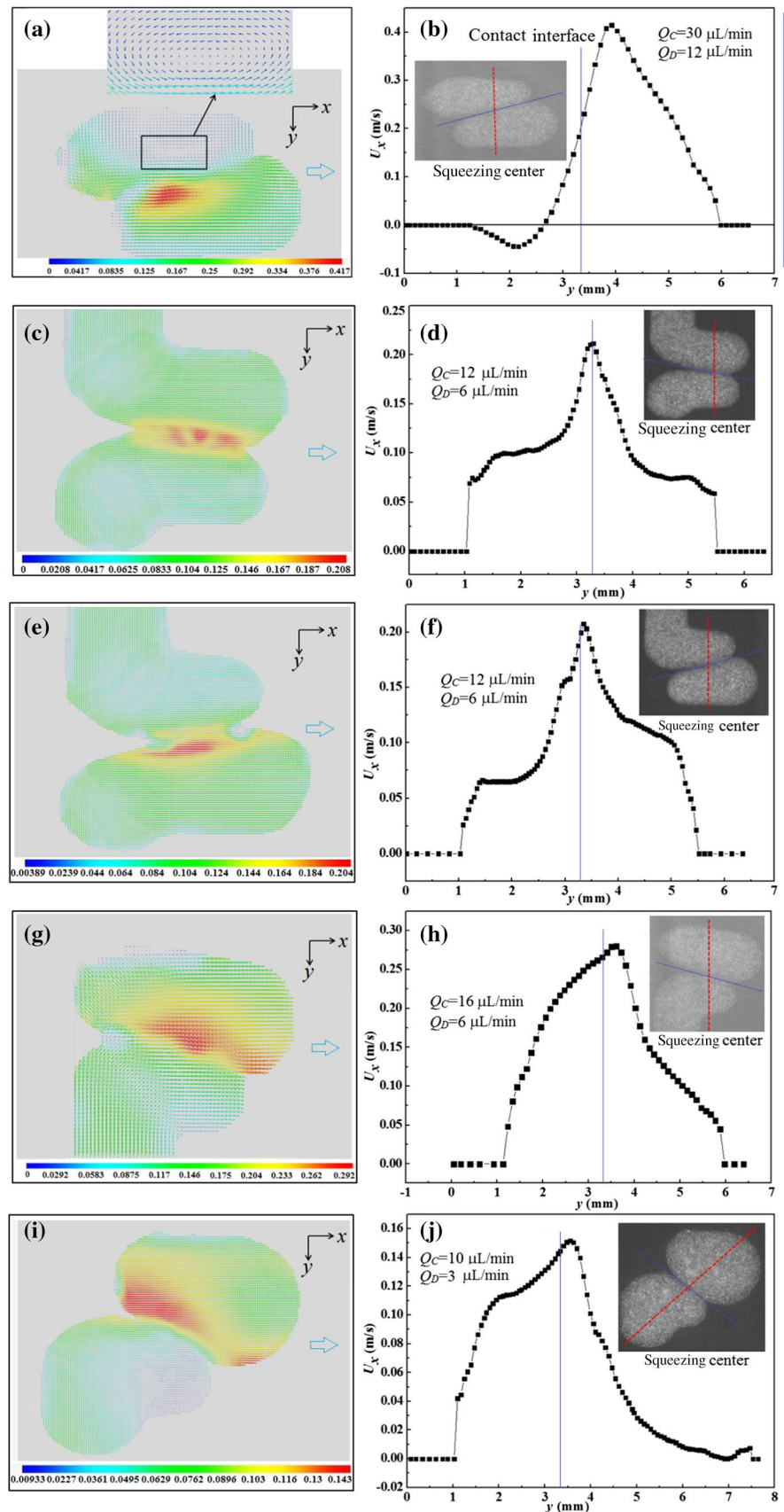
the T-junction was similar to that reported by Wang et al. (2013b), Yang et al. (2012) and Christopher et al. (2009). When the front microdroplet enters the main microchannel (Fig. 3c), due to the sudden broadening of the main microchannel, it will slow down and be squeezed with the later one. If the microdroplets contact time is longer than film drainage time, coalescence occurs finally.

Figure 3d, e show that microdroplets at the T-junction also had good time synchronicity; however, they did not coalesce immediately until they became head-on contact after a longer period of squeezing time in the main microchannel. Under the pressure of the surrounding fluid, the front microdroplets rotated and deformed at the T-junction, which induced the relative movement of the contact surface of the contacting microdroplet. The viscous shearing stress of the moving surface carries the surrounding fluid into the liquid film between the contacting microdroplets, making it

difficult to drain out the liquid film. Currently, most studies on the theory of liquid film drainage focus on head-on contact of round microdroplets (Wang et al. 2013a, Yang et al. 2012; Choi and Lee 2014; Liao and Lucas 2010); rotation of microdroplets has attracted research attention only in a few studies (Wang et al. 2013a).

In order to reveal the microdroplet flow behaviors during coalescence, we employed the micro-PIV system to measure the velocity vector fields inside the microdroplets quantitatively. The velocity vector fields and velocity values for different forms of squeezing coalescence of microdroplets in the T-junction microchannel are shown in Fig. 4 (also enlarged in supplementary Fig. S1). Figure 4a shows that the velocity vector field of two microdroplets at the instant that they just entered the main microchannel and were squeezing each other before merging. It was found that as the upper microdroplets pushed the lower

**Fig. 4** The velocity vector fields and distribution of velocity values for different forms of squeezing coalescences of microdroplets in the T-junction microchannel (enlarged in supplementary Fig. S1). **a, b** Two microdroplets entered the main microchannel before merging. **c, d** Two microdroplets had good time synchronicity of arriving at the main microchannel and squeezed each other. **e, f** Two microdroplets arrived at the main microchannel nearly at the same time. **g, h** The upper microdroplets entered the main microchannel first. The marked red dotted lines located in the corresponding particle images show the velocity distributions  $U_x$ , while the blue straight lines show the  $y$  position of the contact interface



one, the average flow velocity of the lower microdroplet (0.25 m/s) was higher than that of the upper one and the maximum values of the velocity were observed in the left part of the lower microdroplet near the contacting interface. Because of different speeds of the two microdroplets, the surface tension of the lower one induced a shear stress on the upper one, making the appearance of a flow circulation in the upper one, as shown in the enlarged inset in Fig. 4a. Moreover, the velocity value on  $x$  direction ( $U_x$ ) in the center of squeezing location, namely the location of the marked red dotted line in the corresponding particle image (Fig. 4b, inset), was extracted, as shown in Fig. 4b. As the effect of the flow circulation, with the increase in  $y$ , negative value of  $U_x$  appeared and increased at the beginning, then decreased to zero at the center of the circulation. Note that at the position of the interface the velocity value was not zero. This means that the interfaces of the two microdroplets suffered squeezing pressure and shear stress simultaneously. Therefore, the interfaces deformed until the non-uniform surface tension was overcome at the squeezing interface. At the position corresponding to the maximum values of velocity in the lower microdroplet, the  $U_x$  value reached the maximum value (about 0.42 m/s).

Figure 4c shows a situation in which two microdroplets had good time synchronicity of arriving at the main microchannel and squeezed each other. Compared with Fig. 4a, the two microdroplets moved at the same speed and there was no relative movement between them. Therefore, the maximum values of the velocity were near the squeezing area of two microdroplets. Moreover, the distribution of  $U_x$  values, which increased first and then decreased with the  $y$  value increasing (Fig. 4d), is nearly symmetrical with the maximum value of  $U_x$  (0.22 m/s) in the center. The results further prove that there is no shear stress on the interface at this instant. Similar to Fig. 4c, microdroplets in Fig. 4e also arrived at the main microchannel nearly at the same time. Nevertheless, the lower microdroplet entered the main microchannel about 1 ms earlier than the upper one. Hence,

the maximum values of the velocity (0.24 m/s) were in the lower one near the squeezing area, and the right part of the  $U_x$  distribution was higher than the left part of it (Fig. 4f).

In Fig. 4g, i, the upper microdroplets entered the main microchannel first, while the lower ones were still in the T-junction channel. In Fig. 4g, the average flow velocity of the upper microdroplet was 0.20 m/s, which was about 67% higher than that of the lower one (0.12 m/s). In Fig. 4i, the average flow velocity of the upper microdroplets was about 0.13 m/s, which was 1.2 folds higher than that of the lower microdroplets (0.06 m/s). The velocity vector fields show that the maximum values of the velocity were in the area of the upper one near the contacting interface (Fig. 4g, i). Similar results have been reported in our previous study on microdroplet coalescences in Y-shaped microchannels (Liu et al. 2015). In Fig. 4h, j, the distributions of the  $U_x$  values along the marked red dotted line show that the left part of the  $U_x$  distribution is higher than the right part and the highest velocities are 0.28 and 0.15 m/s, respectively. Besides, the microdroplet size and contact angle between them in Fig. 4i were different with that in Fig. 4g. In Fig. 4j, we picked an oblique line perpendicular to the tangent line of the two microdroplets squeezing center, and the range of the  $y$  was extended to 8 mm.

### 3.2 Microdroplet merging in microgrooves

In the microgroove, as the expansion of the main microchannel, the front microdroplet slowed down and contacted the later one. Microdroplet merging in the microgroove also has many forms, which can be summarized into two categories, namely direct head-on coalescence (Fig. 5a) and coalescence after rotation (Fig. 5b). Microdroplets in microgrooves are compressed by the walls of the microfluidic chip, making the liquid film difficult to be drained out than that in macro-scale flow. Many factors can have influence on the occurrence of coalescence, such as the microchannel geometry, the viscosity ratio of two-phase fluids,

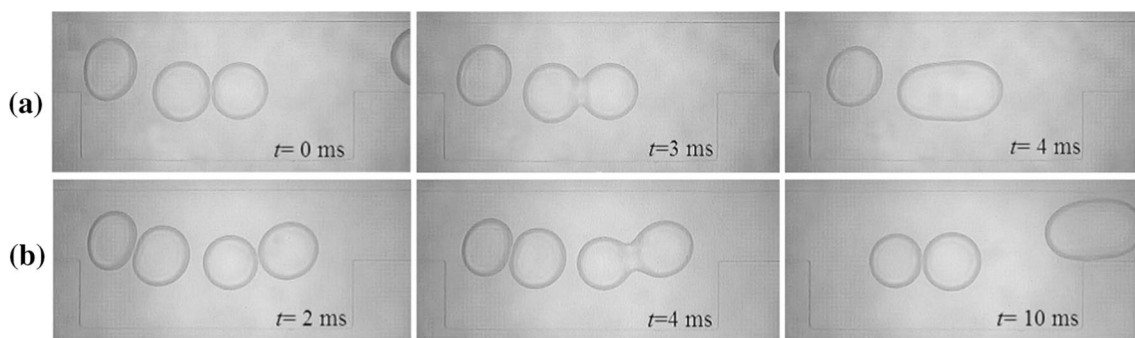


**Fig. 5** Two forms of microdroplet coalescence in microgrooves. **a**  $Q_C = 14 \mu\text{L}/\text{min}$ ,  $Q_D = 4 \mu\text{L}/\text{min}$ ; **b**  $Q_C = 12 \mu\text{L}/\text{min}$ ,  $Q_D = 3 \mu\text{L}/\text{min}$ . The scale bar is 500  $\mu\text{m}$

the diameter of microdroplets, the rotation of the microdroplet and the capillary number ( $Ca$ ) (Wang et al. 2013b; Liao and Lucas 2010).

We explored the velocity vector fields of microdroplets during coalescence in the microgroove, as shown in Fig. 6. It was found that when two microdroplets just contacted each other, the flow velocities around the upper and lower edges of them were relatively high (Fig. 6a). Similar velocity fields were reported by Wang et al. (2013a) for microdroplets collision at a cross-shaped junction. At this instant, the viscous shearing force from the continuous phase made the microdroplets squeeze each other. Moreover, the velocities near the contact area of the two microdroplets are along the tangent line to outside (Fig. 6a), illustrating that the deformation of the microdroplets surfaces accelerates the drainage of the liquid film between them.

Figure 6b shows the velocity vector fields at the beginning instant of coalescence in the microgroove (enlarged in supplementary Fig. S2). It was observed that two symmetric microvortices appeared at both sides of the front one (Fig. 6b, inset). This phenomenon is similar to results in divergent microchannels reported by Jin and Yoo (2012). It was also found that the highest velocities appeared at two points near the merged area between the two microdroplets. Moreover, velocity in the center of the rear microdroplet was higher than that of other areas. The velocity direction in the center of the rear microdroplet was from left to right, while that in the center of the front one was from right to left, which implies that the rear microdroplet was enveloping the front one from outside.

Furthermore, the two-phases flow ratios ( $e$ ) also have significant influences on the coalescence efficiency ( $\eta$ ), as shown in Fig. 7. In the experiments, the microdroplet flow behaviors can only be controlled by varying the two-phase flow rates. It was found that in order to have the occurrence of microdroplets merging, the flow rates of the continuous phase flow should range

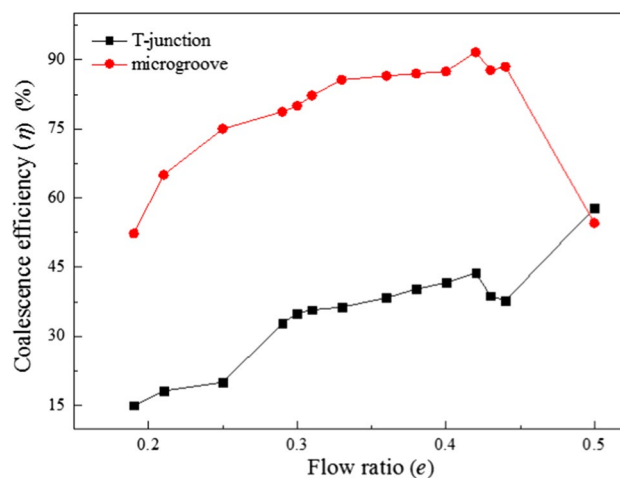


**Fig. 7** The relationship between the coalescence efficiency  $\eta$  and the flow ratios

from 10 to 20  $\mu\text{L}/\text{min}$ . In the T-junction microchannel, coalescence efficiency increases with the increase in  $e$  from 0.18 to 0.5. When  $e$  equals to 0.5,  $\eta$  has the highest value ( $>50\%$ ). In the microgroove, the coalescence efficiency increases first as  $e$  increases from 0.18 to 0.42; then, it decreases with the increase in  $e$  to 0.5. The highest coalescence efficiency ( $\eta = 92\%$ ) comes at  $e = 0.42$  in the microgroove. This is because when the flow ratio is large ( $e > 0.42$ ), the space between nearby microdroplets becomes small, and the front microdroplets may be squeezed out of the microgroove by the later one without coalescence. For both microstructures, the coalescence efficiency is lower when the flow ratio is small ( $e < 0.3$ ) owing to the large spacing of microdroplets. Moreover, the results show that with the increase in  $e$  from 0.18 to 0.5, the probability of the microdroplet coalescence in the microgroove is higher ( $50\% < \eta < 92\%$ ) than that in the T-junction microchannel ( $15\% < \eta < 50\%$ ).

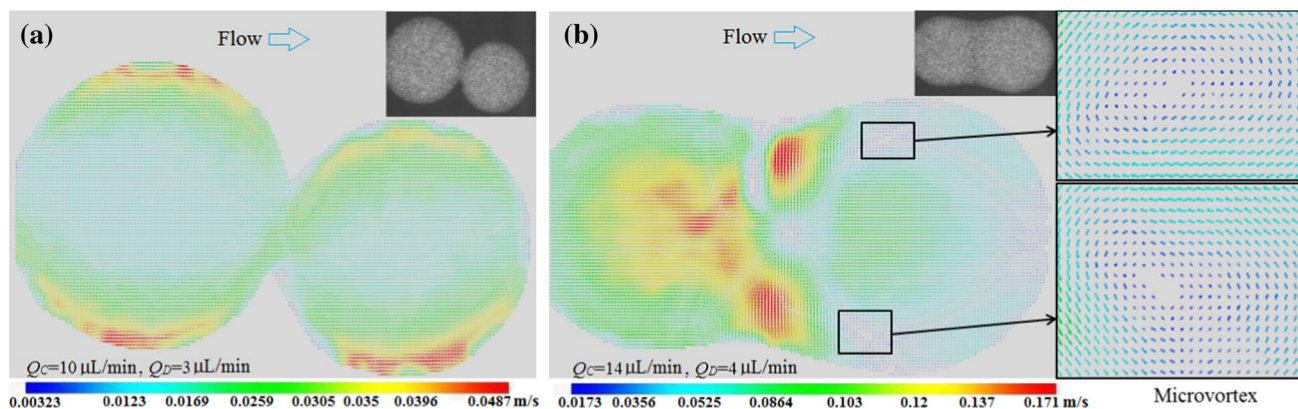


**Fig. 6** The velocity vector fields of microdroplets in the microgroove. **a** Two microdroplets just contact. **b** Coalescence instant



### 3.3 Microdroplets splitting induced by cylinder obstacles

To improve the understanding of microdroplets flow behaviors in confined microstructures, we developed a cylinder obstacle and a Y-junction bifurcation to quantify microdroplet breakup in confined microchannels. Figure 8 shows that the microdroplet dynamic behaviors passing through a cylinder obstacle is very complicated. A microdroplet with a diameter of  $400\ \mu\text{m}$  was split into a big one and a small one after passing the cylinder obstacle (Fig. 8a). At a faster flow rate ( $Q_C = 20\ \mu\text{L}/\text{min}$ ,  $Q_D = 6\ \mu\text{L}/\text{min}$ ), it was split into three ones, and one of them was bigger while the others were very small, as shown in Fig. 8b. This is possibly because the interfacial tension will become unstable with the increase in the flow rate, making the microdroplet split into three parts. Moreover, for column-shaped microdroplets with a larger volume (about  $0.1\ \mu\text{L}$ ) (Fig. 8c, d), they were always split into three ones. The results showed that both the volume of microdroplets and the flow rate have influence on the splitting forms of microdroplets. As the gap is only  $100\ \mu\text{m}$  and much smaller than the diameter of the droplets, the phenomenon that the droplets squeeze through the gap between the obstacle and the microchannel wall was not observed. When passing the cylinder obstacle, the microdroplet deformed significantly under the pressure of the surrounding fluid. A large part of the microdroplet passed the obstacle through the gap. If the pressure gradient overcame the surface tension of the microdroplet, it would break into a large microdroplet first (e.g., Fig. 8a). If the rest part of the microdroplet is still large enough and suffering unbalanced forces, e.g., pressure, viscous shear stress and surface tension, the surface tension will be broke again and the other two small

droplets could be formed (Fig. 8b, c). This phenomenon has not been reported in previous studies (Chung et al. 2010; Li et al. 2014; Protière et al. 2010). Although the cylinder obstacle is symmetrical, the flow field of breakup of the confined microdroplet becomes asymmetric. Note that other physical characteristics of two-phase fluids (e.g., viscosity of fluids, surface tension) may also have effects on the splitting behaviors of microdroplets, which needs further investigation for quantitative data.

For better understanding of the mechanism of these complex phenomena, velocity vector fields of microdroplets passing through the cylinder obstacle were obtained using micro-PIV. For example, Fig. 9a shows that the velocity vector field of a microdroplet passing through a cylinder obstacle was very irregular and many vortices appeared around the obstacle (Fig. 9, inset). In Fig. 9b, the corresponding particle image shows the droplet morphology. As the flow in the microdroplet is unstable, the occurrence of the vortices is random and instantaneous, which will have a significant influence on the microdroplet deformation and make the flow behaviors complicated (Fig. 9a). The dynamics of microdroplet deformation and breakup are usually very complicated for the complex interaction in such a systems (Li et al. 2014; Chung et al. 2010). Until now, due to the non-uniform change of surface tension caused by microdroplet interface deformation and hydromechanics problems induced by transient nonlinear unstable flow of microdroplets, the mechanism of surface breakup near the cylinder obstacle still requires future investigation.

### 3.4 Microdroplets splitting in Y-junction bifurcation

The splitting processes of microdroplets passing through the Y-junction bifurcation are shown in Fig. 10. Due to

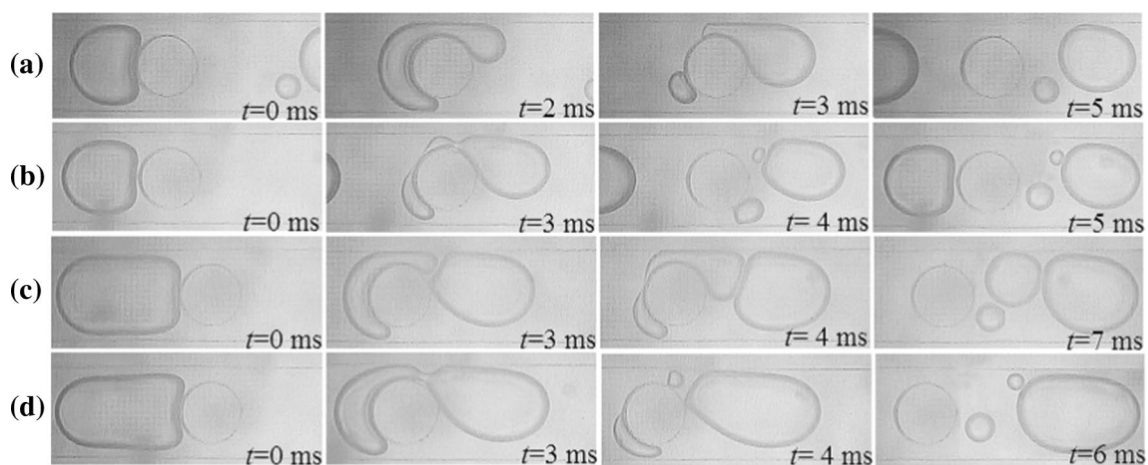


**Fig. 8** Four different splitting forms of microdroplets passing through the cylinder obstacle. **a**  $Q_C = 10\ \mu\text{L}/\text{min}$ ,  $Q_D = 3\ \mu\text{L}/\text{min}$ ; **b**  $Q_C = 20\ \mu\text{L}/\text{min}$ ,  $Q_D = 6\ \mu\text{L}/\text{min}$ ; **c**  $Q_C = 14\ \mu\text{L}/\text{min}$ ,  $Q_D = 4\ \mu\text{L}/\text{min}$ ; **d**  $Q_C = 20\ \mu\text{L}/\text{min}$ ,  $Q_D = 9\ \mu\text{L}/\text{min}$ . The scale bar is  $500\ \mu\text{m}$

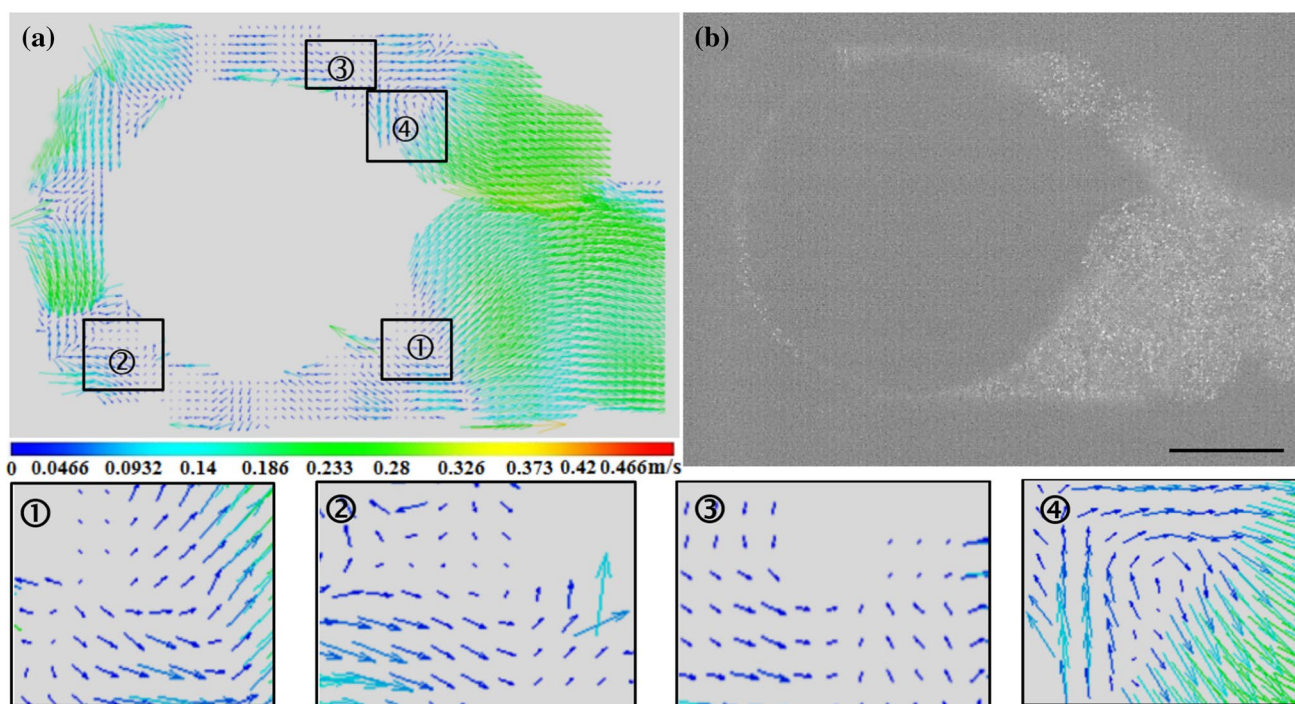


**Fig. 9** **a** The micro-PIV obtained instant velocity vector field and **b** a particle image of a microdroplet passing through the cylinder obstacle at  $Q_C = 30 \mu\text{L}/\text{min}$ ,  $Q_D = 12 \mu\text{L}/\text{min}$ . The *insets* show the microvortices from (a). The *scale bar* is  $100 \mu\text{m}$

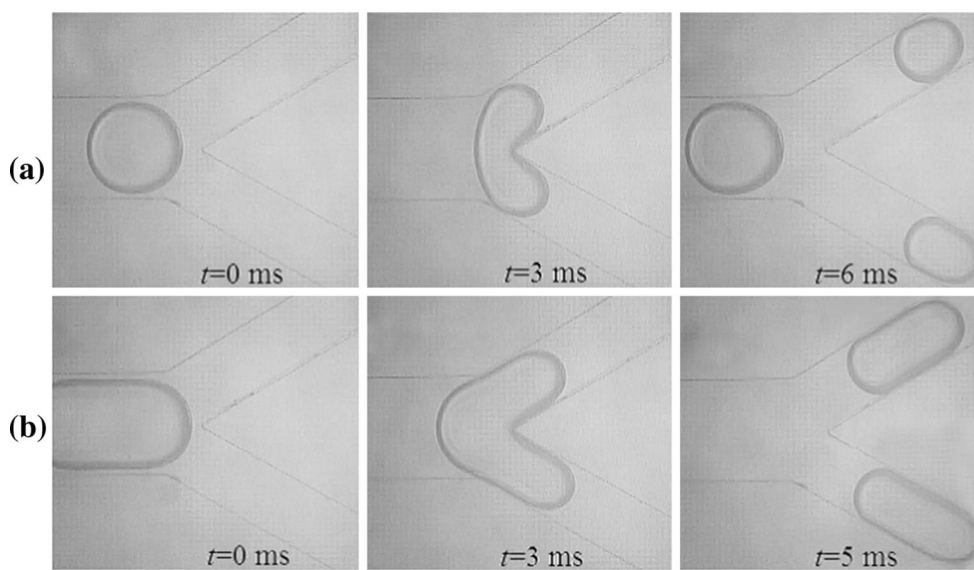


**Fig. 10** Splitting of two microdroplets passing through the Y-junction bifurcation at  $Q_C = 14 \mu\text{L}/\text{min}$ ,  $Q_D = 4 \mu\text{L}/\text{min}$ . **a** Splitting of an unmerged small droplet. **b** Splitting of a merged column-shaped large droplet. The *scale bar* is  $300 \mu\text{m}$

the tip shape and the pressure of the surrounding fluid, the interface of the microdroplet deformed significantly under unbalanced forces. Finally, the pressure overcame the surface tension and the interface split into two parts. In Fig. 10a, an unmerged small microdroplet with a diameter

of  $450 \mu\text{m}$  was split into two smaller ones nearly with the same size with a diameter of  $320 \mu\text{m}$  in the bifurcation. For a merged column-shaped microdroplet with a larger volume of  $0.07 \mu\text{L}$  (Fig. 10b), it was also split into two smaller column-shaped ones with the volume of  $0.03$  and  $0.04 \mu\text{L}$ ,

respectively. In our experiments, the Y-junction bifurcation could split microdroplets (diameter  $>500 \mu\text{m}$ ) with high efficiency ( $\eta > 95\%$ ). However, the sizes of the newly formed microdroplets could not be controlled precisely. We speculate that the slight difference of flow resistance in the downstream induced by surface roughness and geometric deviation of the microchannel may affect the size difference of the newly formed microdroplets. As the flows in the surrounding fluid and the microdroplet are transient and unstable and microdroplet interface deformation may cause non-uniform change of the surface tension, the dynamics of the microdroplet interface splitting is complicated.

Moreover, we used micro-PIV system to measure the flow velocity vector fields of microdroplet splitting in the Y-junction bifurcation (Fig. 11, enlarged in supplementary Fig. S3), which seems to be more regular and stably. However, as the microdroplets were split into two with different sizes, the velocity vector fields of newly formed microdroplets in the bifurcation microchannels were asymmetrical, as shown in Fig. 11. It was also found that the highest velocities occurred at the outside edges of the splitting microdroplets. Meanwhile, the interface on the outside of the splitting microdroplets moved much faster than that on the inside. The results indicate that under the pressure of the continuous fluid, the microdroplet deforms and flows into the bifurcation microchannels. The accelerated fluid near the outside of the splitting microdroplet was driven by the surface tension of the moving interface.

#### 4 Conclusion

The microdroplets merging and splitting in different microstructures were successfully achieved, visualized and

compared by using a high-speed microscope and a micro-PIV system. A T-junction microchannel and a rectangular microgroove were designed to achieve microdroplet merging, and different coalescence forms were observed. Meanwhile, a cylinder obstruction and a Y-junction bifurcation were designed to achieve microdroplet splitting. To better understand the microdroplet flow behaviors, instantaneous velocity vector fields of microdroplets during the merging and splitting processes were measured using the micro-PIV. Velocity distributions were extracted from the squeezing center, and partial view of the velocity vector fields was enlarged to illustrate the existence of microvortices.

In the experiments, different forms of microdroplets merging and splitting induced by different microchannel structures were observed. The results show that the microgroove has a higher probability of microdroplets coalescence than that of the T-junction microchannel, and the highest coalescence efficiency ( $\eta = 92\%$ ) comes at the two-phase flow ratio  $e$  of 0.42 in the microgroove. In the T-junction microchannel, the highest velocities appear near the squeezing area of contacting microdroplets and are affected by the movement of the microdroplets. However, the rear microdroplet envelops the front one during merging in the microgroove and the highest velocities appear at two points on the front one near the merged area. Moreover, velocity vector fields of microdroplets passing through a cylinder obstacle are complex and many microvortices appear. On the contrary, Y-junction bifurcation can split microdroplets into two ones with high efficiency ( $\eta > 95\%$ ) and the microdroplet flow during splitting is steady. The results of the present study can provide better understanding of microdroplet behaviors and useful guidance for the design and fabrication of more efficient microchannel structures for various droplet-based microfluidic chip applications.

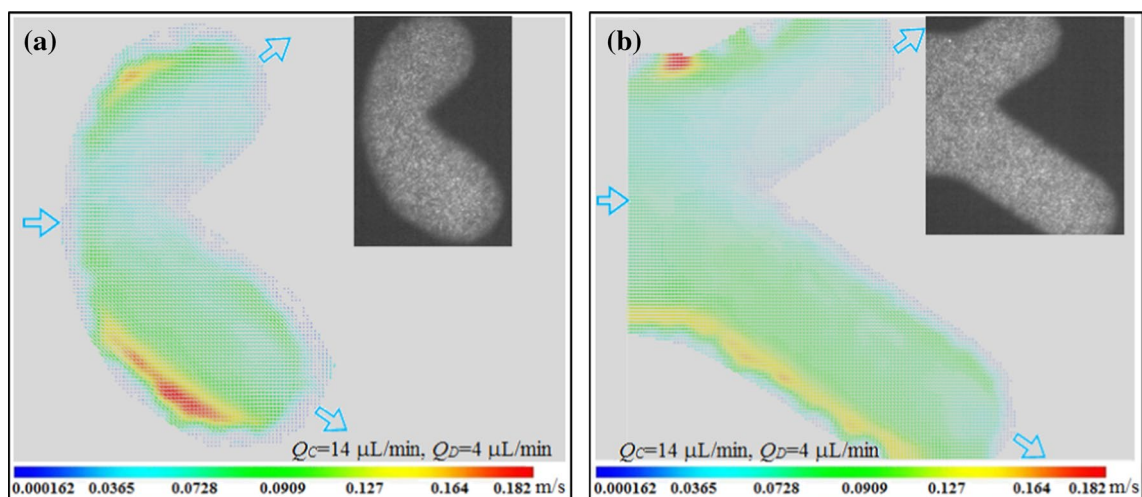


**Fig. 11** The velocity vector fields of two microdroplets splitting through the Y-junction bifurcation (enlarged in supplementary Fig. S3). **a** Splitting of an unmerged small droplet. **b** Splitting of a merged column-shaped large droplet. The arrows show the flow direction

**Acknowledgements** This work was supported by the Beijing Municipal Natural Science Foundation (7152012), General Program of Science and Technology Development Project of Beijing Municipal Education Commission (KM201610005002), Natural Science Foundation of China (11572013), China Scholarship Council (201406545031), Training Plan of New Talent of Beijing University of Technology (2015-RX-L02), NIH (R21AI107415 and SC2GM105584), and the NSF-PREM program (DMR 1205302).

## References

- Abate AR, Hung T, Mary P, Agresti JJ, Weitz DA (2010) High-throughput injection with microfluidics using picoinjectors. *Proc Natl Acad Sci* 107:19163–19166
- Alves SS, Orvalho SP, Vasconcelos JMT (2005) Effect of bubble contamination on rise velocity and mass transfer. *Chem Eng Sci* 60(1):1–9
- Baroud CN, Gallaire F, Dangle R (2010) Dynamics of microfluidic droplets. *Lab Chip* 10:2032–2045
- Chen H, Li J, Shum HC, Stone HA, Weitz DA (2011) Breakup of double emulsions in constrictions. *Soft Matter* 7:2345–2347
- Chen YT, Chang WC, Fang WF, Ting SC, Yao DJ, Yang JT (2012) Fission and fusion of droplets in a 3-D crossing microstructure. *Microfluid Nanofluid* 13:239–247
- Chen YP, Liu XD, Zhang CB, Zhao YJ (2015) Enhancing and suppressing effects of an inner droplet on deformation of a double emulsion droplet under shear. *Lab Chip* 15:1255–1261
- Chen Y, Gao W, Zhang C, Zhao Y (2016) Three-dimensional splitting microfluidics. *Lab Chip* 16:1332–1339
- Choi SB, Lee JS (2014) Film drainage mechanism between two immiscible droplets. *Microfluid Nanofluid* 17(4):675–681
- Chong ZZ, Tan SH, Gañán-Calvo AM, Tor SB, Loh NH, Nguyen NT (2016) Active droplet generation in microfluidics. *Lab Chip* 16(1):35–58
- Chou WL, Lee PY, Yang CL, Huang WY, Lin YS (2015) Recent advances in applications of droplet microfluidics. *Micromachines* 6:1249–1271
- Christopher GF, Bergstein J, End NB, Poon M, Nguyen C, Anna SL (2009) Coalescence and splitting of confined droplets at microfluidic junctions. *Lab Chip* 9:1102–1109
- Chung C, Ahn KH, Lee SJ (2009) Numerical study on the dynamics of droplet passing through a cylinder obstruction in confined microchannel flow. *J Non-Newtonian Fluid Mech* 162:38–44
- Chung C, Lee M, Char K, Ahn KH, Lee SJ (2010) Droplet dynamics passing through obstructions in confined microchannel flow. *Microfluid Nanofluid* 9:1151–1163
- Collignon S, Friend J, Yeo L (2015) Planar microfluidic drop splitting and merging. *Lab Chip* 15(8):1942–1951
- Day P, Manz A, Zhang Y (2012) Microdroplet technology: principles and emerging applications in biology and emerging applications in biology and chemistry. Springer, New York
- Deng NN, Meng ZJ, Xie R, Ju XJ, Mou CL, Wang W, Chu LY (2011) Simple and cheap microfluidic devices for the preparation of monodisperse emulsions. *Lab Chip* 11:3963–3969
- Dietrich N, Poncin S, Midoux N, Li HZ (2008) Bubble formation dynamics in various flow-focusing microdevices. *Langmuir* 24(24):13904–13911
- Dore V, Tsaoulidis D, Angeli P (2012) Mixing patterns in water plugs during water/ionic liquid segmented flow in microchannels. *Chem Eng Sci* 80:334–341
- Dou M, Dominguez DC, Li X, Sanchez J, Scott GA (2014) Versatile PDMS/paper hybrid microfluidic platform for sensitive infectious disease diagnosis. *Anal Chem* 86:7978–7986
- Dou M, Garcia JM, Zhan S, Li X (2016) Interfacial nano-biosensing in microfluidic droplets for high-sensitivity detection of low-solubility molecules. *Chem Comm.* 52(17):3470–3473
- Duffy DC, McDonald JC, Schueller OJA, Whitesides GM (1998) Rapid prototyping of microfluidic systems in poly(dimethylsiloxane). *Anal Chem* 70:4974–4984
- Dutse SW, Yusof NA (2011) Microfluidics-based lab-on-chip systems in DNA-based biosensing: an overview. *Sensors* 11(6):5754–5768
- Duxenneuner MR, Fischer P, Windhab EJ, Cooper-White JJ (2014) Simultaneous visualization of the flow inside and around droplets generated in microchannels. *Microfluid Nanofluid* 16(16):743–755
- Fatoyinbo HO, Labeed FH (2015) Microfluidics in detection science: lab-on-a-chip technologies. Royal Society of Chemistry, Cambridge
- Gijs MAM, Lacharme F, Lehmann U (2010) Microfluidic applications of magnetic particles for biological analysis and catalysis. *Chem Rev* 110(3):1518–1563
- Gu H, Duits MH, Mugele F (2011) Droplets formation and merging in two-phase flow microfluidics. *Int J Mol Sci* 12(4):2572–2597
- Guillot P, Colin A, Ajdari A (2008) Stability of a jet in confined pressure-driven biphasic flows at low Reynolds number in various geometries. *Phys Rev E* 78(1):139–143
- Hoang DA, Portela LM, Kleijn CR, Kreutzer MT, Steijn VV (2013) Dynamics of droplet breakup in a T-junction. *J Fluid Mech* 717(R4):1–11
- Huerre A, Theodoly O, Leshansky AM, Valignat MP, Cantat I, Jullien MC (2015) Droplets in microchannels: dynamical properties of the lubrication film. *Phys Rev Lett* 115:064501
- Jin BJ, Yoo JY (2012) Visualization of droplet merging in microchannels using micro-PIV. *Exp Fluids* 52(1):235–245
- Jin BJ, Kim YW, Lee Y, Yoo JY (2010) Droplet merging in a straight microchannel using droplet size or viscosity difference. *J Micromech Microeng* 20:035003
- Jung JH, Lee KH, Destgeer G, Lee KS, Cho H, Ha BH, Sung HJ (2015) In situ seriate droplet coalescence under an optical force. *Microfluid Nanofluid* 18(5–6):1247–1254
- Kinoshita H, Kaneda S, Fujii T, Oshima M (2007) Three-dimensional measurement and visualization of internal flow of a moving droplet using confocal micro-PIV. *Lab Chip* 7(3):338–346
- Leman M, Abouakil F, Griffiths AD, Tabeling P (2015) Droplet-based microfluidics at the femtolitre scale. *Lab Chip* 15:753–765
- Leshansky AM, Pismen LM (2009) Breakup of drops in a microfluidic T junction. *Phys Fluids* 21:023303
- Li ZH, Wu JK, Hu GQ, Hu GH (2012) Fluid flow in microfluidic chips. Science Press, Beijing
- Li Q, Chai Z, Shi B, Liang H (2014) Deformation and breakup of a liquid droplet past a solid circular cylinder: a lattice Boltzmann study. *Phys Rev E* 90:043015
- Liao YX, Lucas D (2010) A literature review on mechanisms and models for the coalescence process of fluid particles. *Chem Eng Sci* 65:2851–2864
- Lin BC, Qin JH (2008) Graphic laboratory on a microfluidic chip. Science Press, Beijing
- Lindken R, Rossi M, Grosse S, Westerweel J (2009) Micro-particle image velocimetry ( $\mu$ PIV): recent developments, applications, and guidelines. *Lab Chip* 9(17):2551–2567
- Link DR, Anna SL, Weitz DA, Stone HA (2004) Geometrically mediated breakup of drops in microfluidic devices. *Phys Rev Lett* 92(5):054503
- Liu K, Ding H, Chen Y, Zhao X-Z (2007) Droplet-based synthetic method using microflow focusing and droplet fusion. *Microfluid Nanofluid* 3:239–243

- Liu ZM, Cao RT, Pang Y, Shen F (2015) The influence of channel intersection angle on droplets coalescence process. *Exp Fluids* 56(2):1–4
- Loewenberg M, Hinch EJ (1997) Collision of two deformable drops in shear flow. *J Fluid Mech* 338:299–315
- Mai DJ, Brockman C, Schroeder CM (2012) Microfluidic systems for single DNA dynamics. *Soft Matter* 8(41):10560–10572
- Mark D, Haerberle S, Roth G, von Stetten F, Zengerle R (2010) Microfluidic lab-on-a-chip platforms: requirements, characteristics and applications. *Chem Soc Rev* 39(3):1153–1182
- Marques MPC, Fernandes P (2011) Microfluidic devices: useful tools for bioprocess intensification. *Molecules* 16(10):8368–8401
- Moritani T, Yamada M, Seki M (2011) Generation of uniform-size droplets by multistep hydrodynamic droplet division in microfluidic circuits. *Microfluid Nanofluid* 11:601–610
- Mu X, Zheng W, Sun J, Zhang W, Jiang X (2013) Microfluidics for manipulating cells. *Small* 9(1):9–21
- Nghe P, Terriac E, Schneider M, Li ZZ, Cloitre M, Abecassis B, Tabeling P (2011) Microfluidics and complex fluids. *Lab Chip* 11(5):788–794
- Niu X, Gulati S, Edel JB, DeMello AJ (2008) Pillar-induced droplet merging in microfluidic circuits. *Lab Chip* 8:1837–1841
- Oishi M, Kinoshita H, Fujii T, Oshima M (2011) Simultaneous measurement of internal and surrounding flows of a moving droplet using multicolour confocal micro-particle image velocimetry (micro-PIV). *Meas Sci Technol* 22(10):105401. doi:10.1088/0957-0233/22/10/105401
- Pit AM, Duits MHG, Mugele F (2015) Droplet manipulations in two phase flow microfluidics. *Micromachines* 6:1768–1793
- Protière S, Bazant MZ, Weitz DA, Stone HA (2010) Droplet breakup in flow past an obstacle: a capillary instability due to permeability variations. *EPL* 92:54002
- Qi D, Hoelzle DJ, Rowat AC (2012) Probing single cells using flow in microfluidic devices. *Eur Phys J Special Top* 204(1):85–101
- Raven JP, Marmottant P (2006) Periodic microfluidic bubbling oscillator: insight into the stability of two-phase microflows. *Phys Rev Lett* 97(15):13129–13169
- Rosenfeld L, Lin T, Derda R, Tang SKY (2014) Review and analysis of performance metrics of droplet microfluidics systems. *Microfluid Nanofluid* 16:921–939
- Salánki R, Gerecsei T, Orgovan N, Sándor N, Péter B, Bajtaz Z, Erdei A, Horvath R, Szabó B (2014) Automated single cell sorting and deposition in submicroliter drops. *Appl Phys Lett* 105:083703
- Sarrazin F, Loubiere K, Prat L, Gourdon C, Bonometti T, Magnaudet J (2006) Experimental and numerical study of droplets hydrodynamics in microchannels. *AIChE J* 52(12):4061–4070
- Schmid L, Weitz DA, Franke T (2014) Sorting drops and cells with acoustics: acoustic microfluidic fluorescence-activated cell sorter. *Lab Chip* 14:3710–3718
- Schneider T, Kreutz J, Chiu DT (2013) The potential impact of droplet microfluidics in biology. *Anal Chem* 85:3476–3482
- Schoch RB, Han J, Renaud P (2008) Transport phenomena in nanofluidics. *Rev Mod Phys* 80(3):839–883
- Schoeman RM, Kemna EWM, Wolbers F, Berg AVD (2014) High-throughput deterministic single-cell encapsulation and droplet pairing, fusion, and shrinkage in a single microfluidic device. *Electrophoresis* 35:385–392
- Seemann R, Brinkmann M, Pfohl T, Herminghaus S (2012) Droplet based microfluidics. *Rep Prog Phys* 75(1):016601
- Sesen M, Alan T, Neild A (2014) Microfluidic on-demand droplet merging using surface acoustic waves. *Lab Chip* 14(17):3325–3333
- Sharma S, Srisa-Art M, Scott S, Asthana A, Cass A (2013) Droplet-based microfluidics. *Methods Mol Biol* 949:207–230
- Shen F, Li X, Li PCH (2014) Study of flow behaviors on single-cell manipulation and shear stress reduction in microfluidic chips using computational fluid dynamics simulations. *Biomicrofluidics* 8(1):014109
- Shen F, Li Y, Liu ZM, Cao RT, Wang GR (2015a) Advances in micro-droplets coalescence using microfluidics. *Chin J Anal Chem* 43(12):1942–1954
- Shen F, Xiao P, Liu ZM (2015b) Microparticle image velocimetry ( $\mu$ PIV) study of microcavity flow at low Reynolds number. *Microfluid Nanofluid* 19(2):403–417
- Simon MG, Lee AP (2012) Microfluidic droplet manipulations and their applications. In: Day P, Manz Zhang AY (eds) *Microdroplet technology: principles and emerging applications in biology and chemistry*. Springer, New York, pp 23–50
- Song H, Bringer MR, Tice JD, Gerds CJ, Ismagilov RF (2003) Experimental test of scaling of mixing by chaotic advection in droplets moving through microfluidic channels. *Appl Phys Lett* 83:4664–4666
- Squires TM, Quake SR (2005) Microfluidics: fluid physics at the nanoliter scale. *Rev Mod Phys* 77(3):977–1026
- Stone HA, Stroock AD, Ajdari A (2004) Engineering flows in small devices: microfluidics toward a lab-on-a-chip. *Annu Rev Fluid Mech* 36:381–411
- Sun CL, Liu SL (2013)  $\mu$ PIV study of droplet fission in a bifurcating microchannel. In: 10th international symposium on particle image velocimetry-PIV13, pp 1–9
- Sun X, Tang K, Smith RD, Kelly RT (2013) Controlled dispensing and mixing of pico-to nanoliter volumes using on-demand droplet-based microfluidics. *Microfluid Nanofluid* 15(1):117–126
- Tan YC, Fisher JS, Lee AI, Cristini V, Lee AP (2004) Design of microfluidic channel geometries for the control of droplet volume, chemical concentration, and sorting. *Lab Chip* 4(4):292–298
- Teh SY, Lin R, Hung LH, Lee AP (2008) Droplet microfluidics. *Lab Chip* 8(2):198–220
- Timgren A, Tragardh G, Tragardh C (2008) Application of the PIV technique to measurements around and inside a forming drop in a liquid–liquid system. *Exp Fluids* 44(4):565–575
- Wang W, Yang C, Li CM (2009) On-demand microfluidic droplet trapping and fusion for on-chip static droplet assays. *Lab Chip* 9(11):1504–1506
- Wang K, Lu Y, Tan J, Yang BD, Luo GS (2010) Generating gas/liquid/liquid three-phase microdispersed systems in double T-junctions microfluidic device. *Microfluid Nanofluid* 8:813–821
- Wang K, Lu Y, Tostado CP, Yang L, Luo GS (2013a) Coalescences of microdroplets at a cross-shaped microchannel junction without strictly synchronism control. *Chem Eng J* 227(7):90–96
- Wang K, Lu YC, Yang L, Luo GS (2013b) Microdroplet coalescences at microchannel junctions with different collision angles. *AIChE J* 59:643–649
- Wang Y, Wu P, Luo Z, Li Y, Liao M, Li Y, He L (2014) Controllable geometry-mediated droplet fission using “off-the-shelf” capillary microfluidics device. *RSC Adv* 4:31184–31187
- Wang X, Liu GT, Wang K, Luo GS (2015a) Measurement of internal flow field during droplet formation process accompanied with mass transfer. *Microfluid Nanofluid* 19:757–766
- Wang XD, Zhu CY, Wu YN, Fu TT, Ma YG (2015b) Dynamics of bubble breakup with partly obstruction in a microfluidic T-junction. *Chem Eng Sci* 132:128–138
- Whitesides GM (2006) The origins and the future of microfluidics. *Nature* 442(7101):368–373
- Woerner M (2012) Numerical modeling of multiphase flows in microfluidics and micro process engineering: a review of methods and applications. *Microfluid Nanofluid* 12(6):841–886

- Wu HW, Huang YC, Wu CL, Lee GB (2009) Exploitation of a microfluidic device capable of generating size-tunable droplets for gene delivery. *Microfluid Nanofluid* 7:45–56
- Wu YN, Fu TT, Zhu CY, Ma YG, Li HZ (2014) Bubble coalescence at a microfluidic T-junction convergence: from colliding to squeezing. *Microfluid Nanofluid* 8:275–286
- Wu YN, Fu TT, Ma YG, Li HZ (2015) Active control of ferrofluid droplet breakup dynamics in a microfluidic T-junction. *Microfluid Nanofluid* 18:19–27
- Xu B, Nguyen NT, Wong TN (2011) Droplet coalescence in microfluidic systems. *Micro Nanosyst* 3:131–136
- Xu B, Nguyen NT, Wong TN (2012) Temperature-induced droplet coalescence in microchannels. *Biomicrofluidics* 6(1):12811–128118
- Yan Y, Guo D, Luo J, Wen SZ (2013) Numerical simulation of droplet dynamic behaviors in a convergent microchannel. *Biochip J* 7(4):325–334
- Yang L, Wang K, Tan J, Lu YC, Luo GS (2012) Experimental study of microbubble coalescence in a T-junction microfluidic device. *Microfluid Nanofluid* 12:715–722
- Yang SM, Yao H, Zhang D, Li WJ, Kung HF, Chen SC (2015) Droplet-based dielectrophoresis device for on-chip nanomedicine fabrication and improved gene delivery efficiency. *Microfluid Nanofluid* 19(1):1–9
- Yeo LY, Chang H-C, Chan PPY, Friend JR (2011) Microfluidic devices for bioapplications. *Small* 7(1):12–48
- Yoon Y, Borrell M, Park CC, Leal LG (2005) Viscosity ratio effects on the coalescence of two equal-sized drops in a two-dimensional linear flow. *J Fluid Mech* 525:355–379
- Yoon DH, Ito J, Sekiguchi T, Shoji S (2013) Active and precise control of microdroplet division using horizontal pneumatic valves in bifurcating microchannel. *Micromachines* 4(2):197–205
- Zagnoni M, Baroud CN, Cooper JM (2009) Electrically initiated upstream coalescence cascade of droplets in a microfluidic flow. *Phys Rev E* 80(4):593–598
- Zhou B, Wang C, Xiao X, Hui YS, Cao Y, Wen W (2015) Controllable microdroplet splitting via additional lateral flow and its application in rapid synthesis of multi-scale microspheres. *RSC Adv* 5:10365–10371